Sedimentology (1999) **46**, 79–97

The sequence of events around the epicentre of the 1929 Grand Banks earthquake: initiation of debris flows and turbidity current inferred from sidescan sonar

DAVID J. W. PIPER*, PIERRE COCHONAT† and MARTIN L. MORRISON*,‡
**Atlantic Geoscience Centre, Geological Survey of Canada (Atlantic), Bedford Institute of Oceanography, PO Box 1006, Dartmouth, Nova Scotia B2Y 4A2, Canada (E-mail: piper@agc.bio.ns.ca)*
†IFREMER, Géosciences Marines, BP 70, 29280 Plouzané, France
‡Department of Earth Sciences, Memorial University of Newfoundland, St Johns, Newfoundland A1X 3B5, Canada

ABSTRACT

Continental slope sediment failures around the epicentre of the 1929 'Grand Banks' earthquake have been imaged with the SAR (Système Acoustique Remorqué) high-resolution, deep-towed sidescan sonar and sub-bottom profiler. The data are augmented by seismic reflection profiles, cores and observations from submersibles. Failure occurs only in water depths greater than about 650 m. Rotational, retrogressive slumps, on a variety of scales, appear to have been initiated on local steep areas of seabed above shallow (5–25 m) regional shear planes covering a large area of the failure zone. The slumps pass downslope into debris flows, which include blocky lemniscate bodies and intervening channels. Clear evidence of current erosion is found only in steep-sided valleys: we infer that debris flows passed through hydraulic jumps on these steep slopes and were transformed into turbidity currents which then evolved ignitively. Delayed retrogressive failure and transformation of debris flows into turbidity currents through hydraulic jumps provide a mechanism to produce a turbidity current with sustained flow over many hours.

Keywords Debris flow, Grand Banks earthquake, slump, turbidity current.

INTRODUCTION

Purpose

The 'Grand Banks' earthquake of 18 November 1929 on the continental slope south of the island of St Pierre (Fig. 1) caused widespread seabed slumping and initiated a turbidity current that broke cables for up to 13 h after the earthquake (Doxsee, 1948; Heezen & Ewing, 1952; Piper *et al.*, 1988). The general distribution of seabed slumping has been determined from SeaMARC I mid-range sidescan sonar surveys (Piper *et al.*, 1985), but the resolution of this system was insufficient to define many of the failure features. Therefore, in 1990, the IFREMER SAR (Système Acoustique Remorqué) deep-towed, high-resolution sidescan and sub-bottom profiler system was used to investigate particular failure zones on St Pierre Slope (Fig. 2) (Piper *et al.*, 1992; Cochonat & Piper, 1995). The purpose of this study was to determine the morphology and distribution of failure features, in order to better understand the processes leading to sediment failure and the linkage between sediment failure, subsequent evolution of the slide, and finally the initiation of turbidity currents. In ancient rocks, internal structures have been used (Shanmugam *et al.*, 1995; Shanmugam, 1996) to propose that debris flow deposits may be common in expected turbiditic

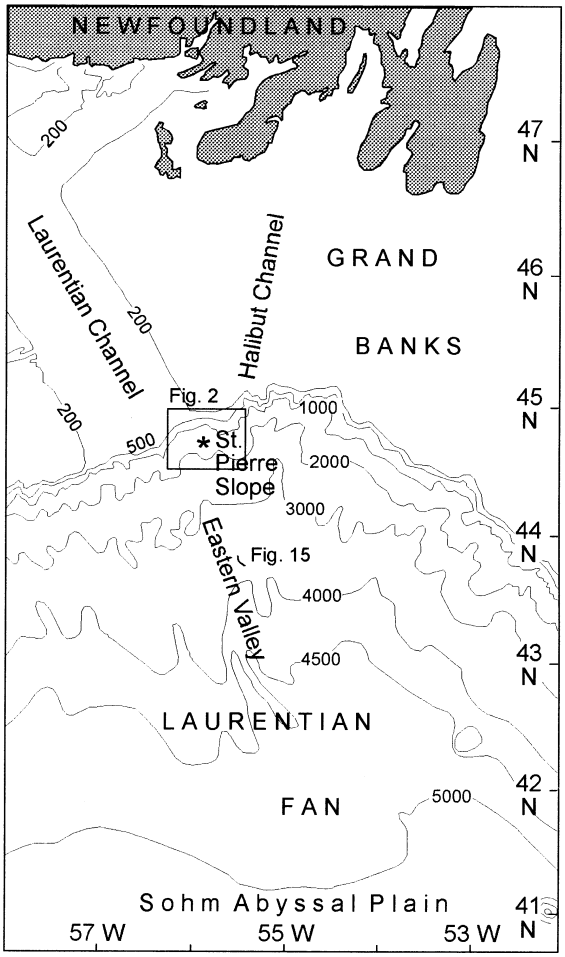

Fig. 1. Regional map showing location of study area and 1929 earthquake epicentre (*).

settings, so defining transitions between different processes occurring in a gravity flow in a modern environment is important.

Geological setting

The St Pierre Slope experienced overall progradation during the Quaternary (Piper & Normark, 1989), but is bounded to the west and east by the major erosional pathways of the Eastern Valley of Laurentian Fan and Halibut Canyon (Fig. 3). Shallow slope valleys, the largest of which (St Pierre Valley) is up to 300 m deep, cut the St Pierre Slope. They probably originated from proglacial erosional processes (Piper, 1988). A prominent bathymetric ridge runs downslope between St Pierre Valley and Halibut Canyon. The upper slope, from the shelf break at approximately 100 m water depth to about 500 m water depth, has a mean gradient of about 2°; below this, the slope steepens to about 5°. The upper slope is underlain by diamicts and sands dating from a late ice advance through Halibut Channel at about 12 ka, overlain by up to 20 m of proglacial sediments and a further 0–6 m of Holocene silty muds that become sandier upslope (Bonifay & Piper, 1988). The diamicts overlie stratified proglacial sediment. On the mid slope, below 500 m water depth, Holocene muds are 1–3 m thick; they overlie a few metres of variegated muds that are the distal equivalent of the upper slope diamicts, and then a thick succession of rapidly deposited muds with scattered ice-rafted gravel dating from about 15 ka and derived principally from glacial outwash down the Laurentian Channel.

The epicentre of the M_s 7·2 'Grand Banks' earthquake of 1929 has been located on the western margin of St Pierre Slope, in about 2000 m water depth. Deep-towed sidescan systems have shown that surface sediments over most of St Pierre Slope show failures, interpreted as rotational slides and debris flow deposits (Fig. 4). The very fresh morphological features suggests that these failures resulted from the 1929 earthquake (Piper *et al.*, 1985; Hughes Clarke, 1990; Piper *et al.*, 1992). These failures show a prominent line of headscarps on the upper slope between 700 and 500 m water depth (large scarps in Fig. 5): above this, sediments appear to have been stable. Some sediments on the ridge between St Pierre Valley and Halibut Canyon were also stable, but generally St Pierre Slope shows a complex of rotational slides, passing downslope into erosional channel systems (Piper *et al.*, 1992) and debris flow deposits (Piper *et al.*, 1985; Hughes Clarke, 1990).

Sidescan imagery (Piper *et al.*, 1985, 1992) shows that pockmarks (gas escape craters) are widespread in undisturbed areas of the slope between 400 and 1700 m water depth, and locally also cut rotational slides. Pockmark abundance is variable, appearing to correlate with the presence of deeper faults. Many cores from St Pierre Slope show gas expansion cracks; gas samples include propane and butane suggesting a petroliferous origin.

The 1929 turbidity current

The behaviour of the turbidity current initiated by the 1929 earthquake has been inferred from cable breaks, the distribution of erosional features, and the character of surficial deposits (Hughes Clarke, 1988; Piper *et al.*, 1988; Hughes Clarke *et al.*, 1990). We suspect that some of the features

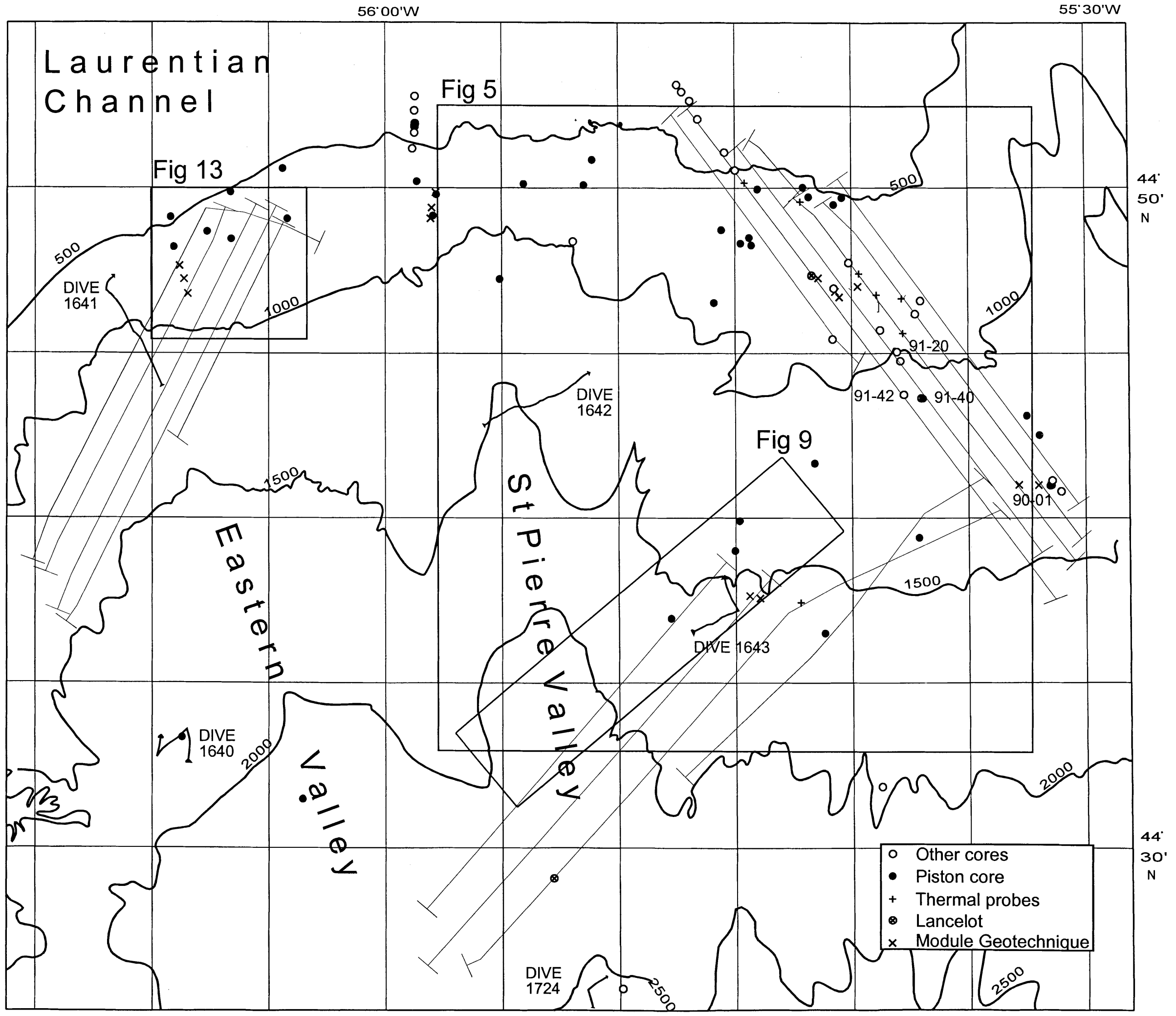

Fig. 2. Map showing available data on St Pierre Slope. Boxes show the location of Figs 5, 9 and 13.

identified by these authors as 1929 deposits, particularly the gravel waves, may be relict late-glacial features, but we interpret erosional forms in sand on the floor of Eastern Valley as resulting from the 1929 event. Cable breaks show that the 1929 current reached velocities of at least 19 m s^{-1} and its flow thickness was of the order of hundreds of metres as determined from erosional trimlines. Total sediment transport is estimated as >150 km^3 from the volume of the deposit on the Sohm Abyssal Plain (Piper & Aksu, 1987). These data imply that the 1929 turbidity current must have flowed for at least 4 h and, more probably, about 11 h (Hughes Clarke, 1988; Piper *et al.*, 1988).

The commonly held model that the current was initiated by a single catastrophic slide or liquefaction event (e.g. Kirwan *et al.*, 1986) is not supported by the data. Seismic or sidescan data show no evidence for a source of liquefied sandy sediment on the continental slope. Observations from submersibles, sidescan sonographs and seismic reflection profiles on the continental slope show little erosion above 1000 m, but increasing amounts of erosion in several different valley systems below that depth. The current accelerated, eroding sediment from the valley floor: it was not a decelerating surge (Hughes Clarke, 1988). We presume a linkage between the widespread failure of muddy sediments on the continental slope and the initiation of the turbidity current, involving mechanisms of the type proposed by Hampton (1972) and Weirich (1989) for the transformation of debris flows into turbidity currents. Currents, once generated, would have accelerated ignitively (Parker, 1982) by erosion of the valley floor. Piper *et al.* (1992) proposed that prolonged retrogressive failure, leading to formation of debris flows and turbidity currents, could have initiated a major ignitive

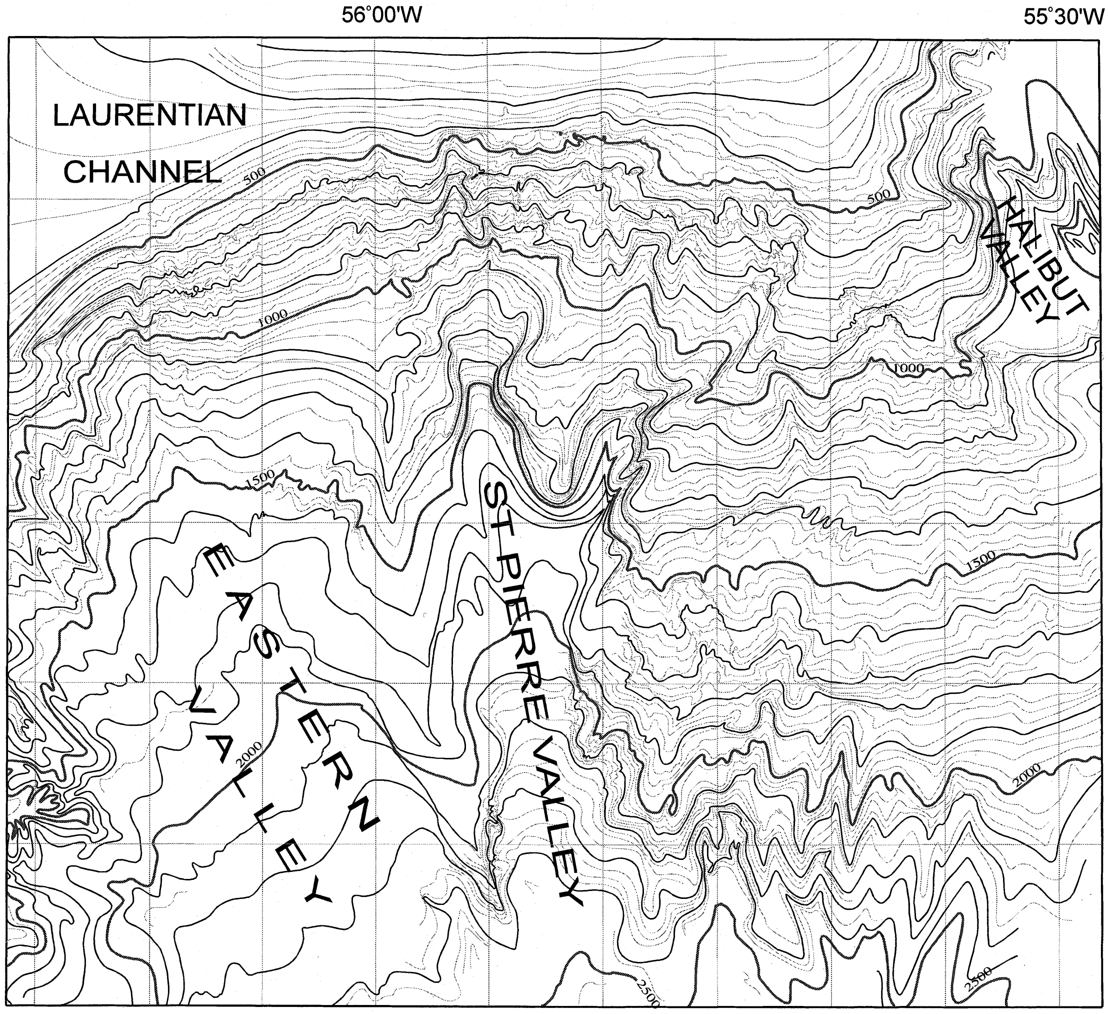

Fig. 3. Bathymetric map of St Pierre Slope near the epicentre of the 1929 earthquake. Based on conventional echo-sounder data, interpolated using sidescan sonographs. The contour interval is 25 m where data permit.

turbidity current over a period of several hours. The detailed evidence for and implications of this concept are examined in more detail in this paper.

METHODS

This study is based on a detailed survey (Fig. 2) using the IFREMER SAR system (Augustin & Voisset, 1989). The SAR is a deep-towed sidescan sonar equipped with 170 kHz (port) and 190 kHz (starboard) transducers and a 3·5 kHz sub-bottom profiler. The system is able to produce a 1500 m wide swath of the seafloor with a pixel size corresponding to a 30 cm^2 footprint. In soft sediments, sub-bottom profiles penetrate the sea floor to a depth of up to 80 m, with a vertical resolution of about 75 cm. All data are digitally recorded and reprocessed in mosaic form with some image enhancement using TRIAS software (Augustin & Voisset, 1989). Navigation was by Global Positioning System (GPS) for about 15 h per day and LORAN-C at other times. The SAR fish was positioned relative to the ship by acoustic ranging. Line drawing interpretations have been prepared for the entire SAR survey (Fig. 5), based both on SAR data and supporting data discussed below.

At the same time as the SAR survey, a 40 cubic inch (655 cm^3) sleeve gun source was used to obtain seismic reflection profiles. Huntec DTS high-resolution boomer profiles of the survey area were obtained on a subsequent cruise in 1991. Cores have been obtained on various cruises within the study area; further ground truth is available from four submersible dives in 1985 (Hughes Clarke *et al.*, 1989) and further dives in 1986 (Fig. 2). The initial selection of SAR survey areas was based on 1983 and 1984 SeaMARC I

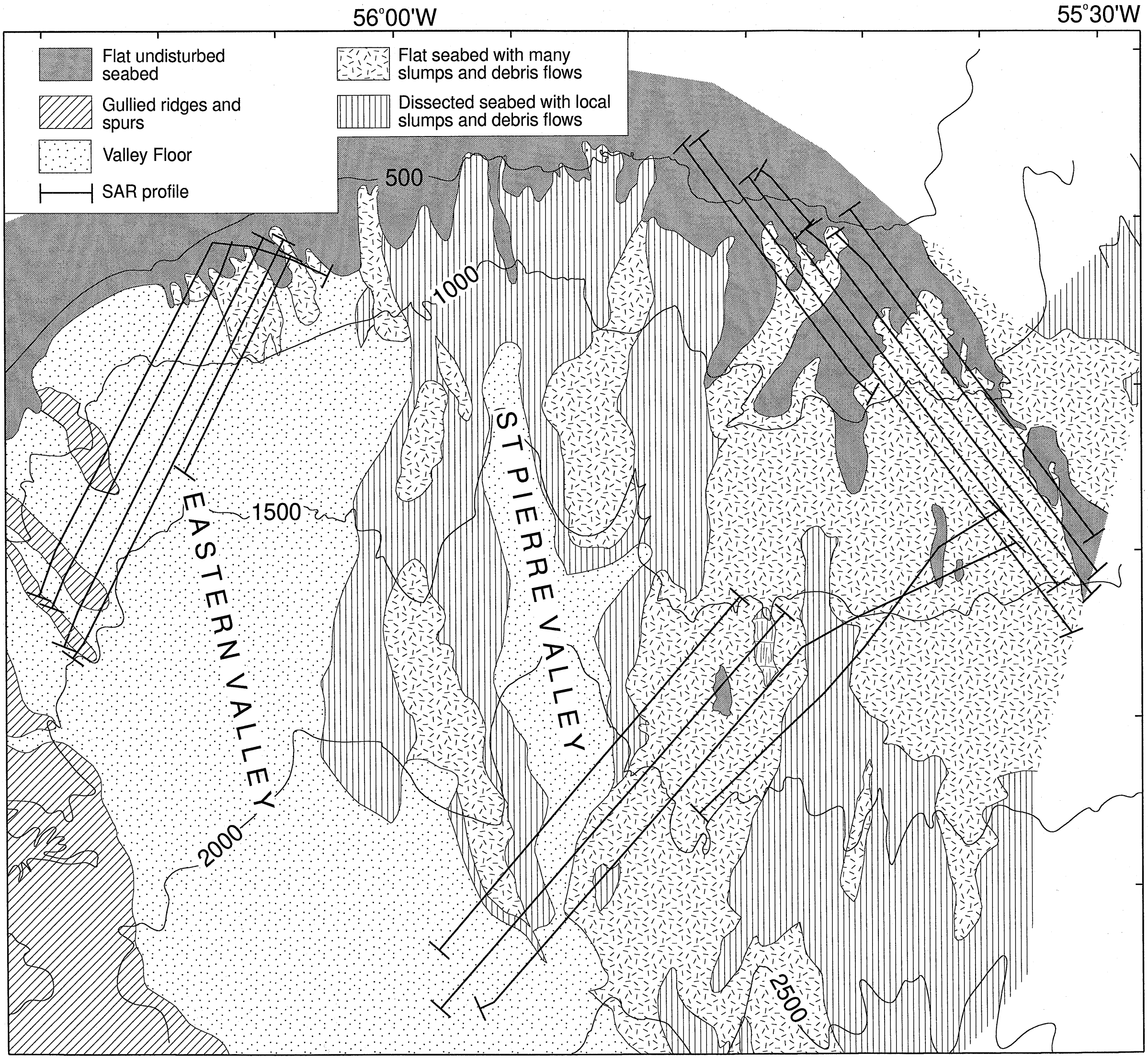

Fig. 4. Interpretative regional map of seafloor facies, based largely on SeaMARC I mid-range sonographs (see Piper *et al.*, 1985) with additional interpretation from new SAR data and facies interpreted from 3·5 kHz profiles. Figure also shows the location of new SAR profiles.

5 km swath sidescan surveys (Piper *et al.*, 1985; Hughes Clarke, 1987). Bathymetric data from these and subsequent sampling cruises have been assembled to produce the new bathymetric map shown in Fig. 3.

Description of seabed facies

Undisturbed seabed

The upper continental slope, to water depths of about 500 m, shows no evidence for sediment failure in either seismic reflection profiles or sidescan sonar imagery. The seabed in places appears smooth; in places, there is evidence of partially buried iceberg scours in water depths as great as 630 m. In many areas, gas escape craters (pockmarks), 30–50 m in diameter, are common (Fig. 6). Isolated 'islands' of undisturbed sediment are also visible in seismic profiles and sidescan imagery down to water depths of 2000 m (Fig. 5).

Rotational slumps

Rotational slumps are visible in sidescan imagery as a series of sub-parallel arcuate ridges (Figs 6–11). These occur at two main scales: small rotational slumps involve failure of sediment 2–5 m thick (Fig. 7) and ridges are spaced a few tens of metres apart (Figs 7, 8). Small rotational

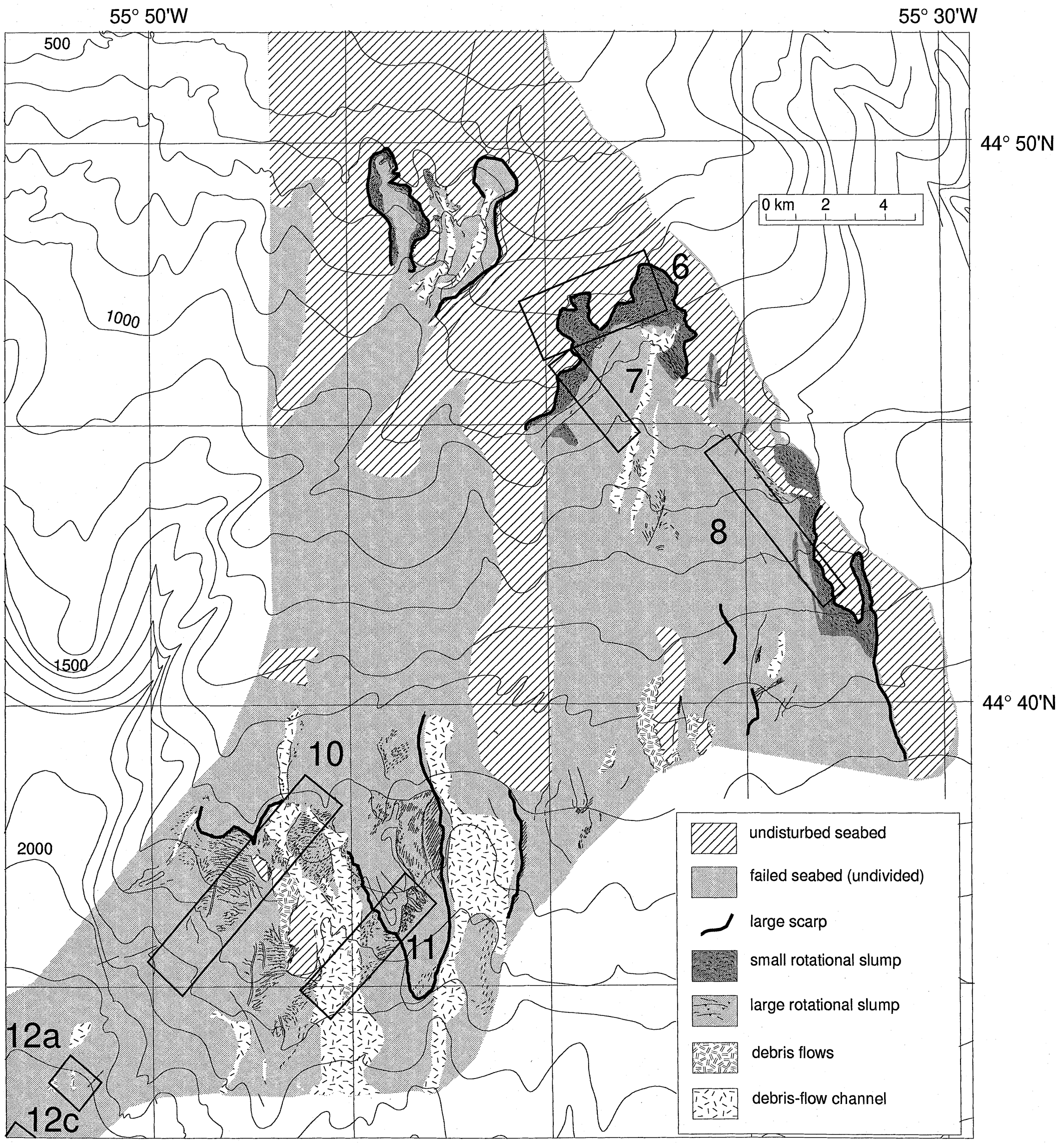

Fig. 5. Detailed line drawing interpretation of sediment failure features on St Pierre Slope. The boxes show the location of Figs 6–8 and 10–12.

slumps commonly terminate laterally against shear zones that are almost orthogonal to slump ridge crests (Fig. 8). The trace of these shear zones can be followed into the slump zone itself. According to the stratigraphy of Bonifay & Piper (1988), small rotational slumps involve only Holocene sediments. They are typically developed on gradients of 2–3°. In some areas, pockmarks clearly cut the small rotational slumps (Fig. 6).

Larger-scale rotational slumps (Figs 8–11) involve failure of sediments 5–30 m thick, with spacing of rotational block crests of > 50 m. Morphologically, they are similar to the small rotational slumps, with the development of orthogonal shear zones.

Ground truth is provided by Pisces dive 1643 (Hughes Clarke *et al.*, 1989), which crossed ridges 5–15 m high, spaced at 200 m, with some bedding inclined at up to 60°. Fresh surfaces indicate that some minor failure may be continuing at present. Talus spalling off these scarps into depressions forms poorly sorted mud clast conglomerates that are probably indistinguishable from debris flow deposits in cores. Headwall scarps were observed on this dive and on dive 1641 (Hughes Clarke *et al.*, 1989).

Debris flow deposits

On sidescan sonar, debris flow deposits have an irregularly textured appearance, lacking strong

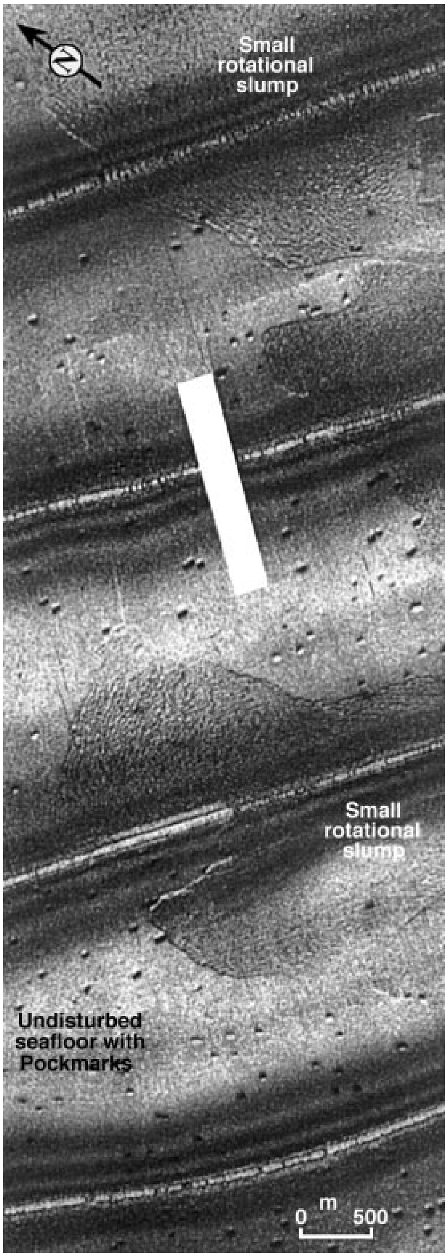

Fig. 6. SAR sidescan image from the upper St Pierre Slope showing abundant pockmarks both outside and within small-scale slumps. The figure location is shown in Fig. 5.

linear features; sub-bottom profiles show acoustically transparent sediment bodies with positive relief. Ground truth is provided by cores 90-01, 91-20 and 91-40, all of which show muddy blocks of sediment on a variety of scales set in a muddy matrix.

Debris flow deposits occur in at least two settings. They are common immediately downslope from the rotational slump facies (Fig. 7), in places partially masking large slump ridges (Figs 10, 11). In this setting, it is in places difficult to distinguish slump and debris flow facies. Cores that contain muddy blocks may represent either true debris flow deposits or talus derived from rotational blocks. Thus the large rotational slumps appear to pass progressively downslope into debris flow deposits.

Debris flow deposits are also common within St Pierre Valley: in places, multiple deposits appear to be stacked. Some flow deposits have strong surface lineations, others are smooth (Fig. 12). The snout of one such flow was investigated on Alvin dive 1724 (Mayer & Halter, unpublished report): the snout was in places steep and 1–2 m high, but elsewhere gradational. Indurated mud clasts were locally visible on the surface of the flow. A pore-pressure probe penetration of the same flow deposit recovered some gravelly sandy mud.

Eroded bedding planes over subsurface inclined zones

In places, rotational slumps pass downslope into elongate zones of eroded seabed in which the gradient is locally steeper (6–10°). This steepening of the dip of surficial sediments in these zones (Fig. 7) mimics that of deeper reflectors which overlie buried faults, old scarps or channel margins.

In sidescan imagery, these zones show erosion down to one or more prominent bedding planes and a lack of surficial deposits. Downslope lineations, probably reflecting erosional furrows cutting the bedding planes, are common. In one area, there is an arcuate depression near the base of the erosional slope that passes downslope into a debris flow channel: this feature appears more like an arcuate rotational slump than a flute-like scour (cf. Shor *et al.*, 1990).

Debris flow channels

Debris flow channels are shallow erosional features less than 20 m deep developed in surficial sediments (Figs 7, 8). Characteristically, the channels are floored by an eroded bedding plane. Some erosional valley sides have only a thin hemipelagic veneer (core 91-42) whereas others are capped by thin debris flow deposits (core 91-40).

On Pisces dive 1643 (Hughes Clarke *et al.*, 1989), a narrow channel between large rotational ridges was crossed (Fig. 10c). It lay at the base of steep 20 m high cliffs. The gully floor was covered with mud, but showed low relief lineations parallel to the length of the gully.

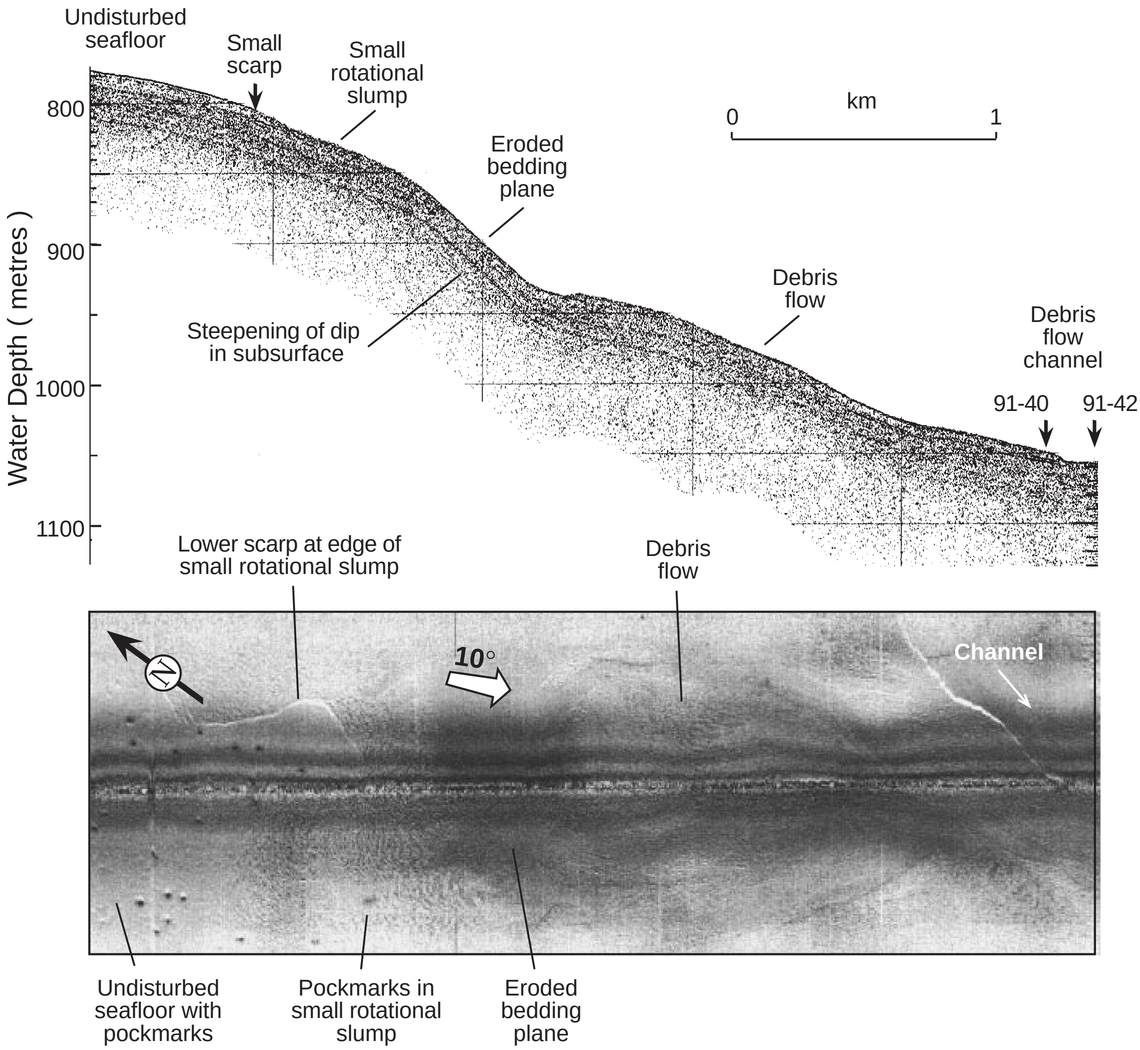

Fig. 7. Sub-bottom 3·5 kHz profile and corresponding SAR sidescan image showing pockmarked undisturbed sediment cut by a small-scale rotational slump which passes across an exposed 10° bedding plane slope into a debris flow with a channel. The figure location is shown in Fig. 5. 91-40 and 91-42 are projected positions of cores.

Valleys: erosional features

Valleys are defined as substantially deeper and wider erosional features than channels. They commonly have a complex facies distribution on their flat floor and indurated sediments outcrop on the valley walls, which are commonly tens to hundreds of metres high. Around the epicentre of the 1929 earthquake, there are at least three types of valley.

1 Eastern Valley of the Laurentian Fan is up to 25 km wide and heads on the steep continental slope (Fig. 3). A portion of the upper part of the valley has been imaged by SAR (Figs 13, 14). Regional coverage of the valley is available from SeaMARC images (Piper *et al.*, 1985), which showed that lineations (apparently erosional in origin) are common above 1600 m; below that, the valley is floored by gravel. The SAR data from the head of Eastern Valley show that large rotational slumps (Fig. 14a) pass rapidly downslope over 2–4 km through a zone of anastomosing channels and residual blocky debris flow deposits (Fig. 14b) into a zone of linear erosional features, apparently linear outcrops of prominent bedding planes (Fig. 14c).

2 St Pierre Valley is a few km wide and heads in a series of scarps at about 600 m water depth on St Pierre Slope (Fig. 4). The middle reach of the valley has been imaged by SAR: it shows areas of erosional lineated valley floor, in places overlain by debris flow deposits, some of which themselves show erosional lineations (Figs 5, 12), indicating further erosion by currents. The walls

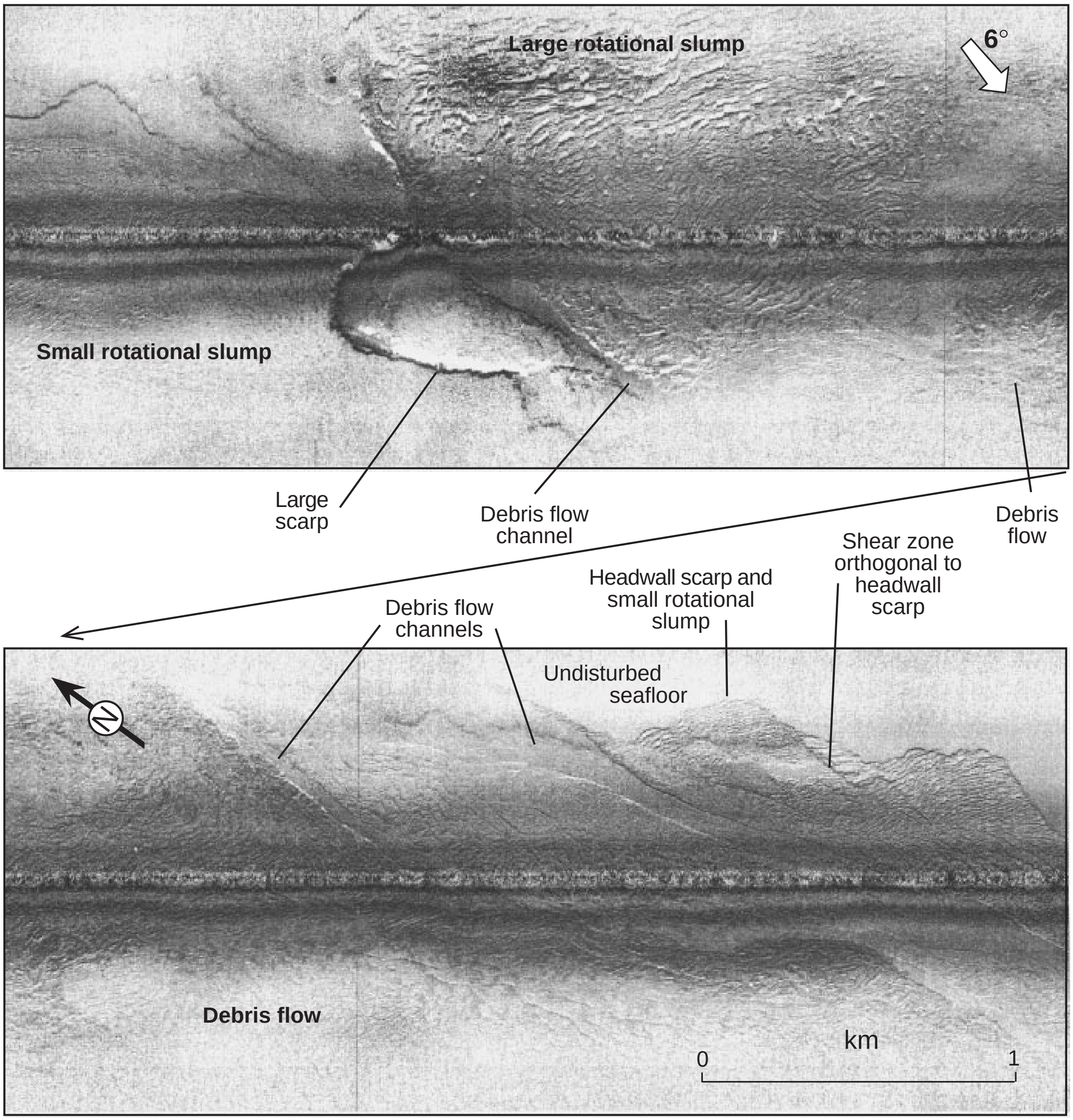

Fig. 8. SAR sidescan image of small- and large-scale rotational slumps on mid St Pierre Slope. The figure location is shown in Fig. 5.

of this part of St Pierre Valley show ridge and gully morphology (Figs 9, 10, top left).

3 A series of smaller valleys east of St Pierre Valley head in water depths of about 2000 m on lower St Pierre Slope (Fig. 3). They have not been imaged by SAR and are poorly imaged by SeaMARC. They are typically 200 m deep and 2 km wide and seismic facies suggest that they are floored by coarse sediment.

Some ground truth for valley flow facies is available from Pisces dives (Fig. 2) (Hughes Clarke *et al.*, 1989). On dive 1642, lineated terrane on the floor of St Pierre Valley was crossed. Lineations consisted of linear ridges 0·4–1·5 m high and spaced at 5–7 m cut into stiff mudstone. Some ridges formed terraces, implying outcropping bedding planes. On dive 1641 in Eastern Valley, outcropping bedding planes and elongate low scour depressions were observed.

Depositional facies in Eastern Valley

SAR imagery has been obtained for parts of Eastern Valley that are floored by gravel waves and sand ribbons, previously observed in SeaMARC images (Piper *et al.*, 1985; Hughes Clarke

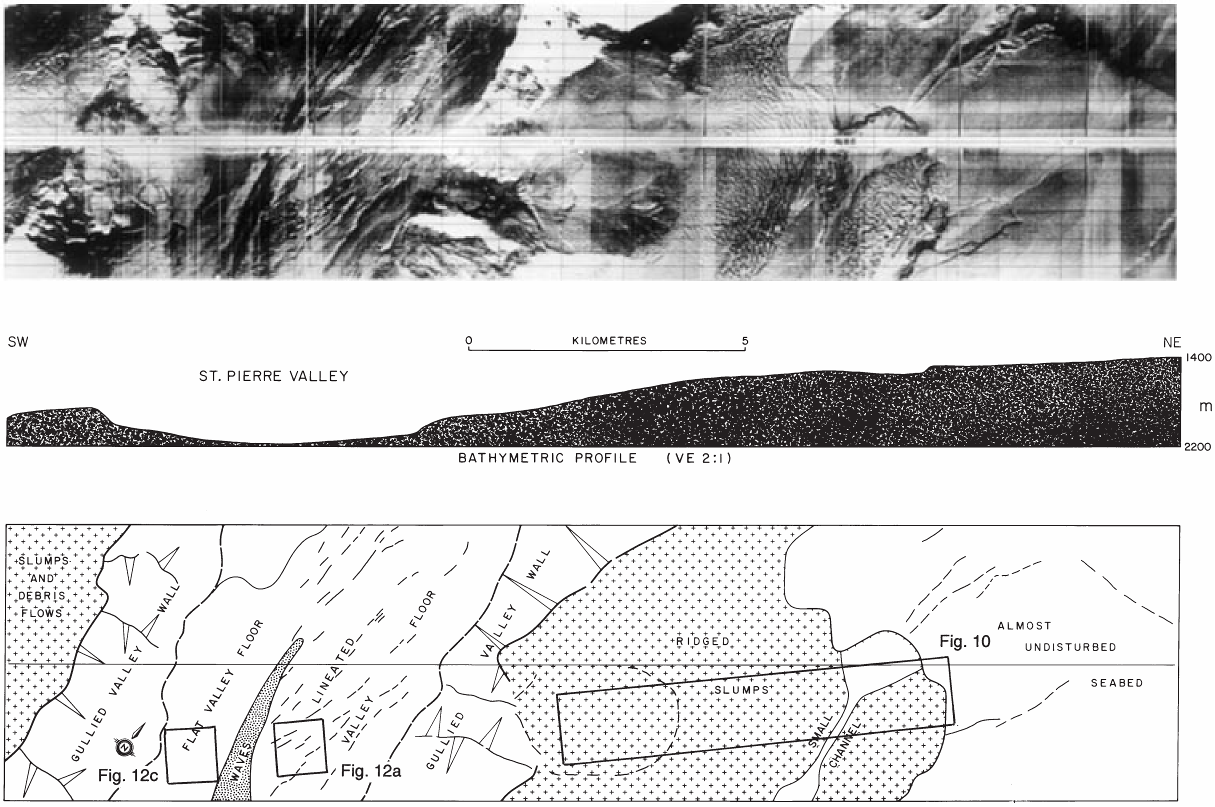

Fig. 9. SeaMARC I image showing sequence of sediment failure on lower St Pierre Slope and the location of Figs 10, 12a and 12c.

et al., 1990). The SAR sub-bottom profiles (Fig. 15) show that the sand ribbons are up to 8 m thick. Whether these features date from 1929 or are older late-glacial deposits is uncertain.

Regional distribution of seabed facies

Middle St Pierre Slope

The middle part of St Pierre Slope, in water depths of 700–1400 m, is characterized by widespread sediment failure in the form of rotational slumps and debris flows (Fig. 5). The process of failure is clearly rotational slumping for each individual failure, but there are many successive overlapping slumps (cf. Mulder & Cochonat, 1996) that retrogressed over a widespread shear plane appearing at a shallow depth below the sea floor (generally <25 m). The value of <<0.15 for the Skempton ratio (Skempton & Hutchinson, 1969) between the depth and length of the slide shows that the overall process is that of a translational slide involving numerous thin-skinned failures.

Between 700 and 900 m water depth, failure appears to have been initiated at a local increase in gradient, where sub-bottom reflections dip at 10°, compared with 3° further upslope (Fig. 7). Small-scale rotational slumps retrogressed upslope from this zone, but stopped in water depths of about 700 m (Fig. 7). There is no gradient change that might be responsible for this upslope limit of failure, but upslope sediments have a higher proportion of silt and fine sand and thus a higher density and permeability.

A zone of undisturbed sediment extends along the crest of the ridge between Halibut Valley and St Pierre Valley to a water depth of at least 1400 m (Figs 4, 5). The western margin of this zone is marked by a series of small-scale rotational slumps. Further downslope, a later large-scale retrogressive slump appears to have been initiated at a local increase in gradient to 6° (Fig. 8). Downslope from these rotational slumps are ribbons of debris flow deposits, shallow debris flow channels, and zones of further retrogressive small-scale rotational slumps. At least 7 km of retrogression can be demonstrated from our side-scan images, and taking into account correlative features imaged on the lower slope, 20 km of retrogression appears probable.

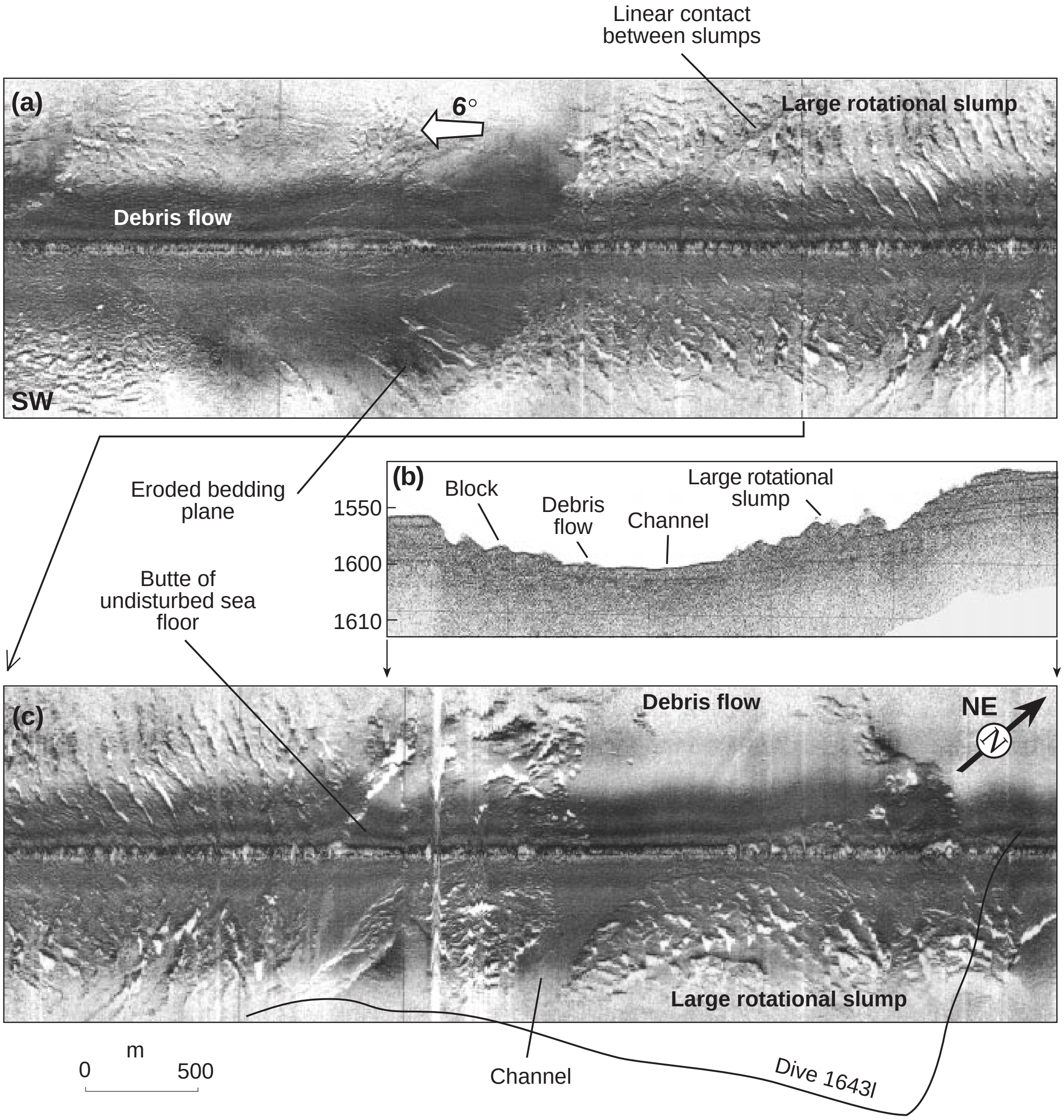

Fig. 10. SAR sidescan image (a, c) of large-scale rotational slumps and debris flows on lower St Pierre Slope and 3·5 kHz SAR profile of part of the image (b). The figure location is shown in Fig. 5. Prominent ridges mark rotational slumps that have retrogressed northward. Note the linear contact between two rotational slumps. In the north-eastern part of the image, rotational slumps have formed a prominent valley north-west of a butte of undisturbed strata, within which a debris flow with a smooth surface has been deposited and partially masks the rotated blocks. The smooth seabed in the north-east of the image has had a few metres of surface sediment removed. In the south-western part of the image, a local steepening of the slope to 6° corresponds to a zone in which underlying strata have been eroded. Downslope from this are blocky debris flow deposits.

Lower St Pierre Slope

The dominant features in 1400–1900 m water depth (Fig. 5) are a series of large rotational slumps, with subparallel ridge crests terminating against or offset by orthogonal shear zones (Figs 9–11). 'Islands' of intact sediment remain that did not form large rotational slumps (Fig. 10b,c). In many cases, these have small rotational surface slumps (Fig. 11), but isolated patches of completely undisturbed seabed remain. These occur at the margin of the large rotational slumps, and the small rotational slumps also show a bending of ridge crests near the edge of the large rotational slumps (Fig. 11).

Downslope from the eastern part of the failure zone, a significant channel is developed within the rotational slumps. This channel cuts down

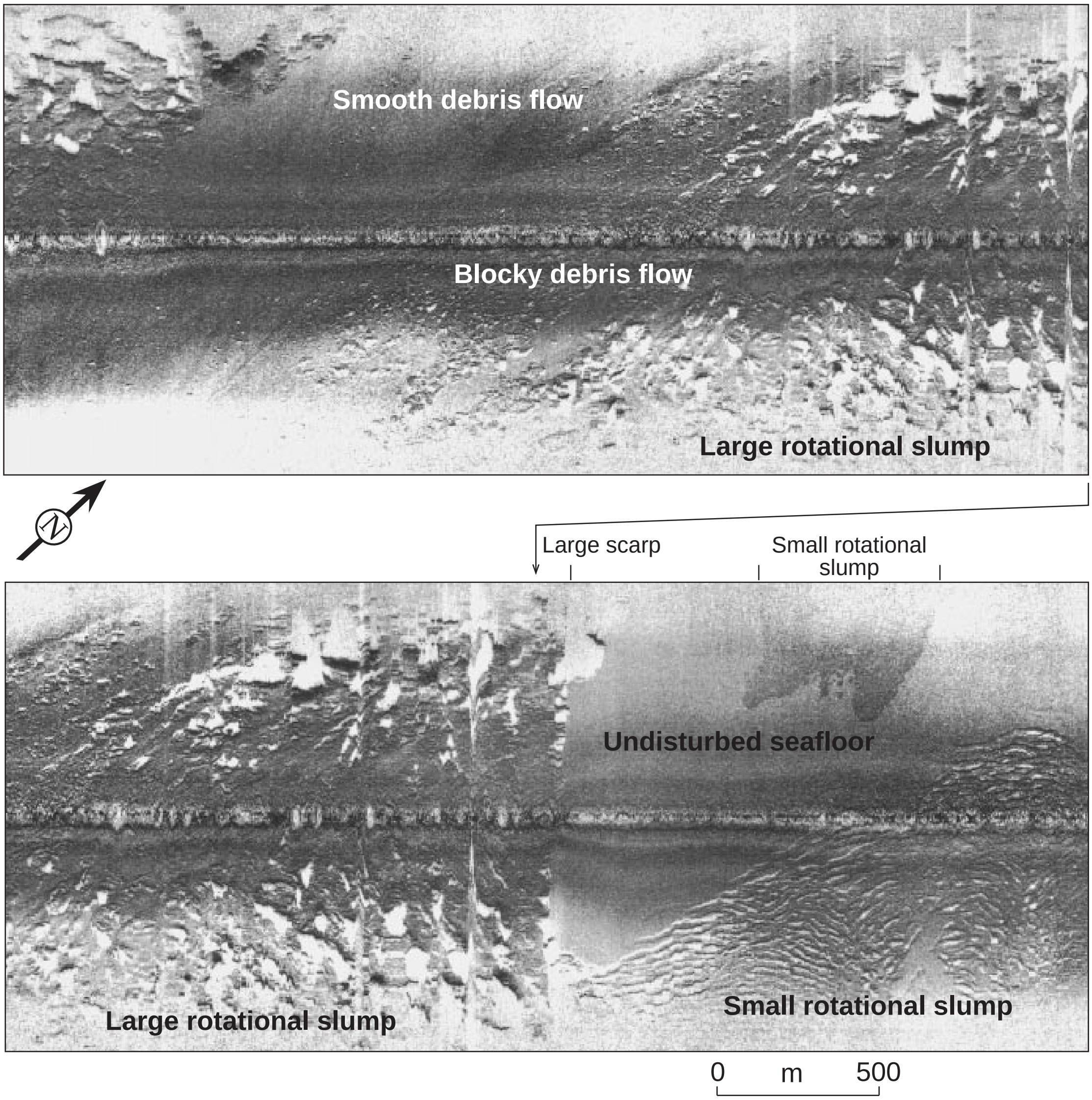

Fig. 11. SAR sidescan image of a large-scale rotational slump overlain by a debris flow deposit that is in places blocky and in places smooth. This is a continuation of the debris flow deposit in Fig. 10. To the north-east is an apparently later small-scale rotational slump. The figure location is shown in Fig. 5.

into sediments slightly below the basal shear plane of the large rotational slumps (Fig. 10b). A transition is seen across the channel from rotated blocks to debris flow deposits with rare blocks to smooth debris flow deposits. In the southern part of the channel, there are subtle lineations on the debris flow and on the lower part of the rotated block field; upstream to the north no evidence for lineations is seen on the SAR images although lineations were observed from submersibles. This channel system appears to lead to deeper valleys to the south that are known from Huntec boomer profiles.

In the western part of the large rotational slump, at the edge of St Pierre Valley, the slump ridges are clearly truncated by a zone of exposed bedding planes (Figs 9, 10a). Ridges to the west appear less sharp, as if partially masked by sediment or partially eroded, and in places, seabed textures typical of debris flow deposits are seen. The debris flow area is cut by shallow channels. SAR images indicate downslope trending ridges in the steeper bedding plane zone, which are similar to the feature on mid St Pierre Slope. This feature may be interpreted as some form of avalanching or glide failure down a steep slope. Downslope, the surficial sediments are interpreted as principally debris flow deposits that locally mask remnants of large rotational slumps. They have an average gradient of only

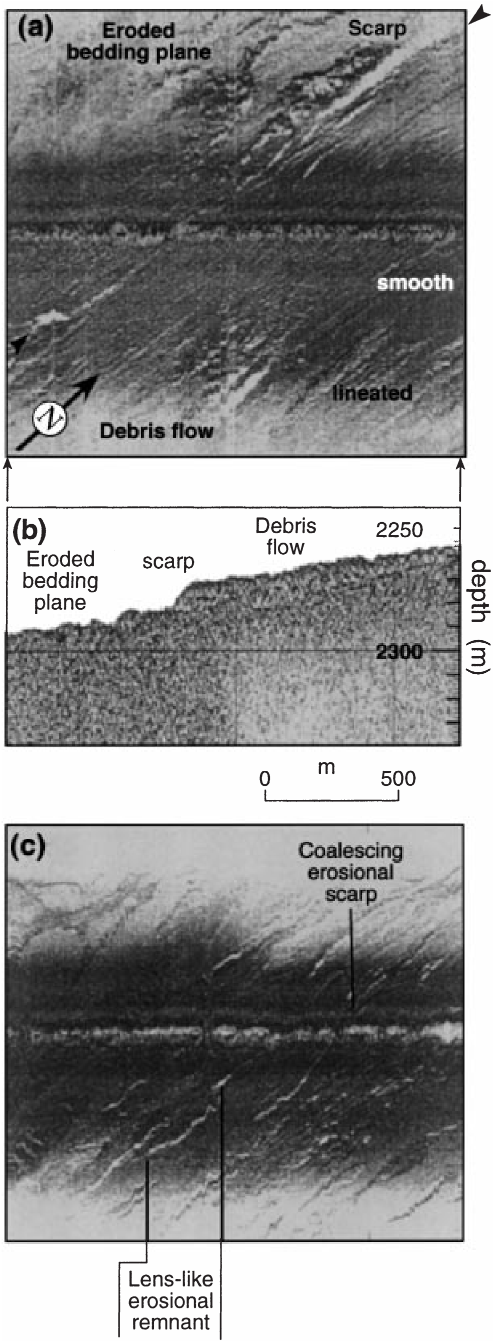

Fig. 12. SAR sidescan images and sub-bottom profile from the floor of St Pierre Valley. (a) Sidescan image of debris flow with prominently lineated surface apparently overlying smooth debris flow. The margin of debris flow is marked by a scarp (arrows), with eroded valley floor to the north-west. (b) Corresponding 3·5 kHz sub-bottom profile of the image (a) showing the 10 m thick debris flow deposit. (c) Sidescan image of the eroded valley floor immediately west of image (a). Note lens-like erosional remnants and coalescing erosional scarps along bedding planes.

1·5°, but pass downslope into steep ridge and gully topography on the walls of St Pierre Valley with mean gradients of 3–5° (Fig. 9). The debris flows on the floor of St Pierre Valley (Fig. 12) have a limited north–south extent and appear to be derived from transport down the Eastern Valley wall.

Upper Eastern Valley

At the head of Eastern Valley, the regional gradient is about 6°, considerably steeper than on St Pierre Slope, with local gradients as steep as 9°. Undisturbed sediment with some pockmarks is found to water depths of about 500 m, similar to the maximum depth at which till has been recognized in sub-bottom profiles (Bonifay & Piper, 1988). Large headscarps 20–25 m high (Fig. 14a) cut the entire stratified sediment sequence above till. Downslope, a few large-scale rotational slumps are preserved. The slumps pass rapidly downslope into debris flow deposits, and, within a few kilometres, grade into seabed consisting of eroded bedding planes (Fig. 14c). Near the headscarps, rotational slump blocks appear partially buried by debris flow material (Fig. 14a), both smooth and blocky, as observed on St Pierre Slope (Figs 11, 12). In general, two debris flow facies are distinguished. Planform lenses of acoustically transparent material 6–10 m thick show a rough surface in sonar images and are interspersed with shallow anastomosing channels that appear to contain smooth debris flow material (Figs 13, 14b). In places, blocks emerge from these smooth debris flows. It is difficult to precisely identify the downslope limit of the channels, but they appear to debouch onto eroded bedding planes, in places with isolated blocks, that downslope pass into a zone with linear bedding plane scarps (Fig. 14b), trending perpendicular to the isobaths, similar to those identified in St Pierre Valley (Fig. 12c). This transition from headscarps to eroded valley floor takes place over a distance of only 4–5 km, in contrast to the much longer distances (20–35 km) on St Pierre Slope.

Synthesis of the sequential evolution of debris flows and turbidity currents

The sequence of failure events imaged in this study must be interpreted within the context of the style of the 1929 turbidity current (Piper *et al.*, 1988; Hughes Clarke, 1988). This current travelled at a velocity that peaked at more than 19 m s^{-1} and deposited >150 km^3 of sediment on

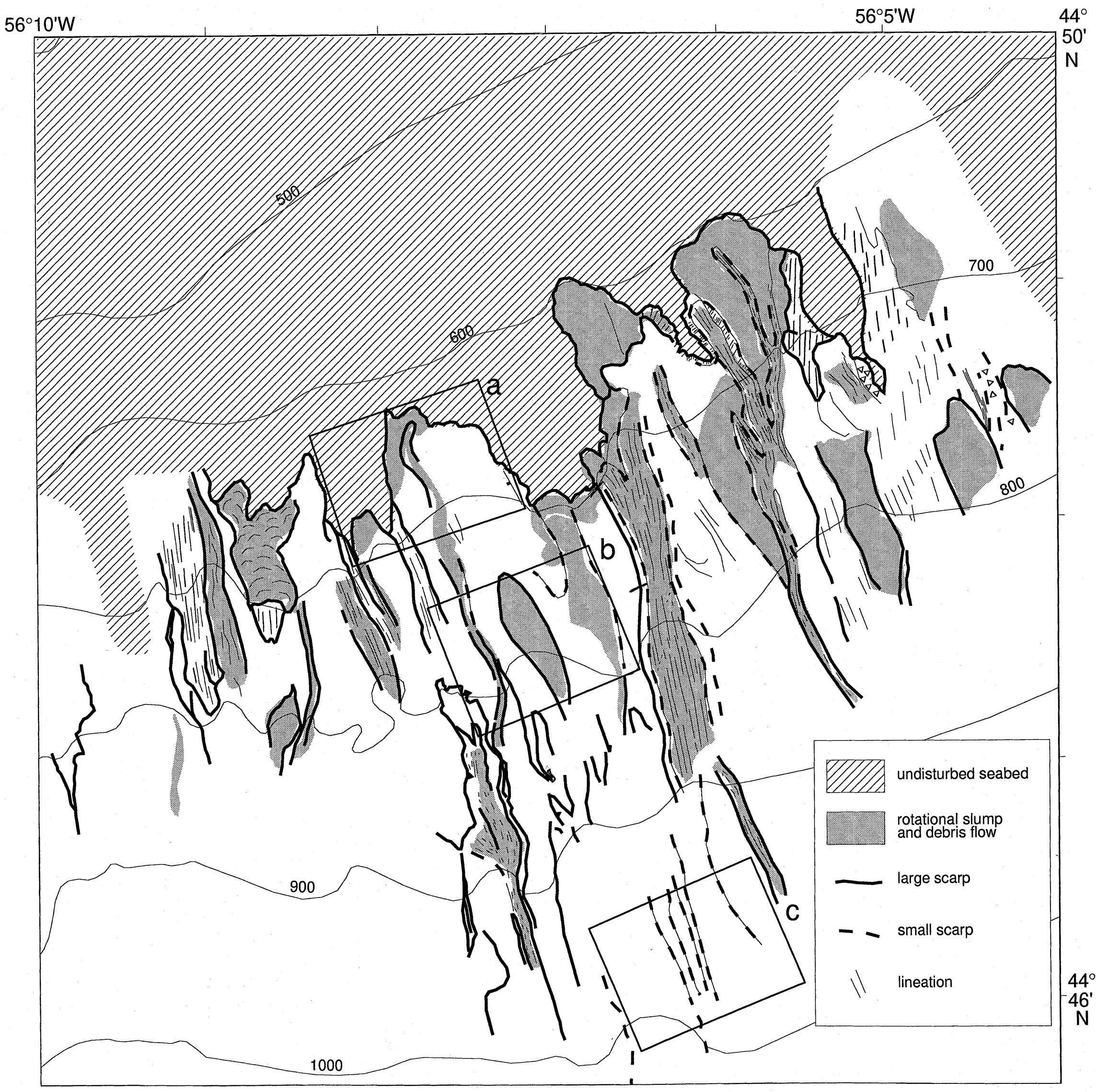

Fig. 13. Line drawing of a mosaic of sidescan images of the upper part of Eastern Valley, showing transition from headwall scarps through debris flows to an extensive zone of erosion. Boxes are the locations of Fig. 14(a)–(c).

the Sohm Abyssal Plain. Mass balance calculations show that most of this sediment was sand, presumably eroded from the floors of the fan valleys, rather than muds derived from slope failure (Piper & Aksu, 1987). Using reasonable limits for the density of this turbidity current, Hughes Clarke (1988) estimated a duration of flow of at least 4 and probably 11 h.

According to our new SAR data, there is no evidence for deep failure of a large sediment body at the head of Eastern Valley that might be considered the source of the 1929 turbidity current. Rather, there has been widespread failure on the continental slope of a surficial layer 20–25 m thick of proglacial stratified sediment. This confirms previous interpretations made from SeaMARC imagery (Piper *et al.*, 1985) and submersible dive 1641 (Hughes Clarke *et al.*, 1989).

How then did the rotational slumps observed on the continental slope lead to the formation of a major turbidity current of considerable duration? The change in seafloor morphology downslope provides a general interpretation of the processes involved (Fig. 16). The upper and mid-slope areas are dominated by rotational slumps that appear to lead downslope into debris flows. St Pierre Valley, Eastern Valley and the steep-sided valleys of lower St Pierre Slope all show predominantly erosional features or are floored by sorted gravel. Debris flow deposits are rare in these valleys. There is thus presumably a transition from debris

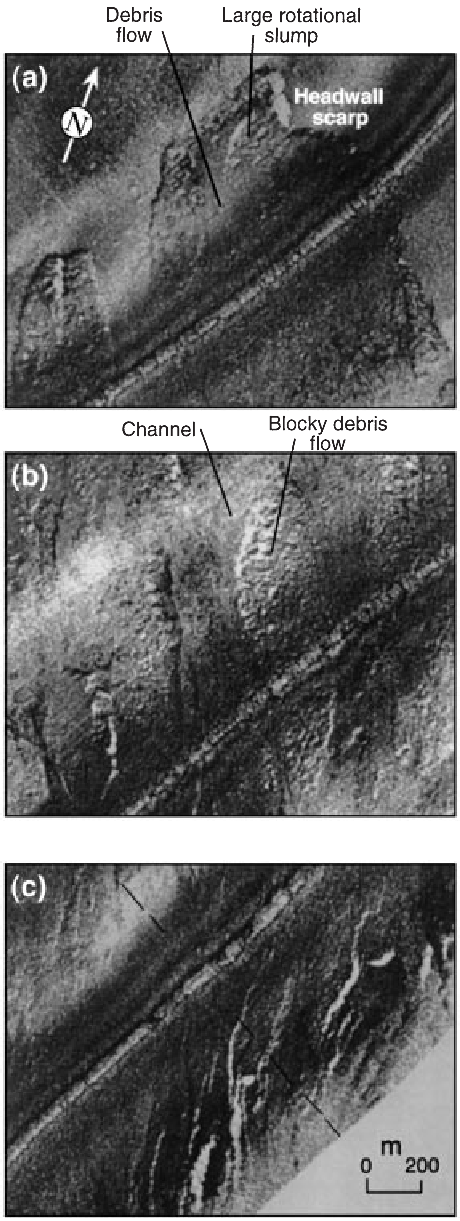

Fig. 14. Detailed sidescan images, showing (a) headwall scarps and large-scale rotational slumps, partially buried by debris flow deposits, (b) blocky debris flow deposits 6–10 m thick separated by anastomosing channels with thin smooth debris flow deposits, and (c) erosional seabed with linear bedding-plane scarps.

flows to turbidity currents in water depths of 700–1500 m on the continental slope.

Experimental work by Hampton (1972) has shown that erosion of the upper interface of a debris flow will produce a turbidity current; this process is more effective on steep slopes and in muddier flows. Alternatively, in-mixing of water at the base of a debris flow may result in whole-flow transformation of the flow into a turbidity current (Allen, 1971). This whole-flow transformation has been observed on steep slopes in lakes where a debris flow goes through a hydraulic jump (Weirich, 1989). A suspension current on a steep slope may be sufficiently powerful to erode bed sediment and thus increase in size and velocity: a condition described as ignition (Parker, 1982). Hughes Clarke *et al.* (1990) proposed that talweg channels up to 40 m deep on the floor of Eastern Valley represented the main sites for ignitive erosion of sediment.

The morphological freshness of the slumps, their similar regional extent to the instantaneous cable breaks, the lack of overlying hemi-pelagic sediment, and the lack of similar sub-bottom failures all indicate that they were formed during the 1929 Grand Banks earthquake (Piper *et al.*, 1985). Slumps appear to have been initiated in local steeper zones by earthquake shaking and then progressively retrogressed upslope (Fig. 16). Since excess pore pressure sustains low sediment strength during failure and movement, the bending of ridge crests in small rotational slumps near the edge of the large rotational slumps (Fig. 11) suggests that drainage of sediment adjacent to the large slumps stabilized the seabed and that the small slumps post-date the large slumps. Drainage of sediments may also be responsible for the upslope limit of retrogressive small rotational slumps on the upper slope.

Downslope break-up of rotational slumps to form mudslides (*sensu* Brunsden, 1984) or debris flows is indicated by the present morphology, with debris flow deposits and shallow channels present immediately downslope from steeper zones and many large rotational slumps. Conversion of rotational slumps to debris flows would be most rapid on steep slopes. Such transitions are well-known on many continental slopes (e.g. Hesse & Klaucke, 1995; Mulder *et al.*, 1997). There is no evidence for significant turbidity current erosion in the main zone of slumps and debris flows on St Pierre Slope. In the area illustrated in Fig. 10, for example, break-up of rotated blocks appears to have formed a debris flow, part of which was deposited at the margin of the channel, but most of which flowed across the lower part of the block field and right out of the area, leaving an exposed bedding plane at the base of the channel. There is no positive evidence for erosion by currents, and evidence of any form of upstream erosion is lacking. None of the debris flow channels shows evidence for vigorous erosion, they lack coarse sediment, and many have low levees constructed of debris flow sediments.

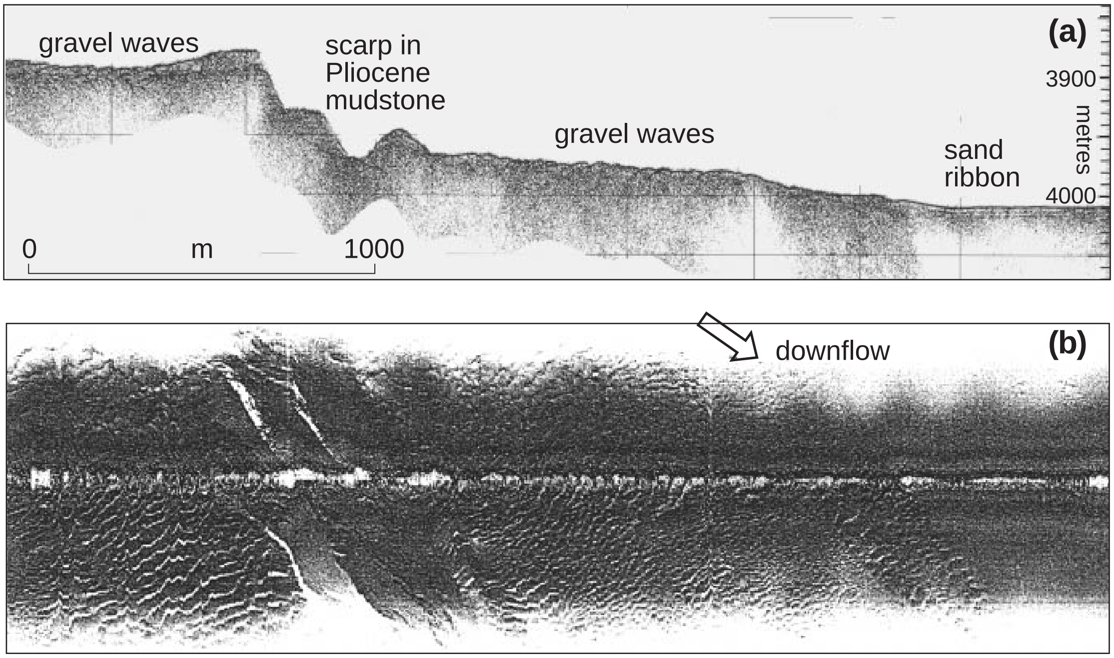

Fig. 15. SAR sidescan image and subbottom profile showing transition from erosional remnant to valley floor of Eastern Valley. Note well-developed gravel waves on and downstream from the erosional remnant, that are onlapped by coarse sand sheets. The figure location is shown in Fig. 1.

Thus they appear to represent pathways of flow of more fluid threads of debris flows. Erosion is commonly down to a particular bedding plane, which may represent the regional horizontal shear plane forming the base of the numerous rotational failures in the retrogressive slumps. The planform lenses of more blocky debris flow material resemble frozen slugs of the type described by Johnson & Rodine (1984) from Klare Springs, California.

A suite of erosional and depositional features at 2300 m in St Pierre Valley suggests that by this position, turbidity current flow had developed. These features include sand or gravel waves, the streamlined form of bedding plane erosion on the valley floor, and erosional lineations on the surface of debris flows.

In St Pierre Valley, the abrupt change in gradient at steep valley walls (> 6°) would provide ample opportunity for a hydraulic jump and break up of debris flows entering from St Pierre Slope (Fig. 17). The lack of thick debris flow deposits at the head of Eastern Valley also points to the break-up and transformation of debris flows there on slopes of 6–9°. In this area, changes in gradient are gradual and there is no evidence of flute-like scours that might be evidence of a hydraulic jump. The development of a turbidity current may have taken place through a process of whole-flow entrainment of water and progressive change from a fluid debris flow into a turbidity current.

We thus interpret that pre-existing relief played an important role in the initiation of the 1929 turbidity current from failure of muddy sediment

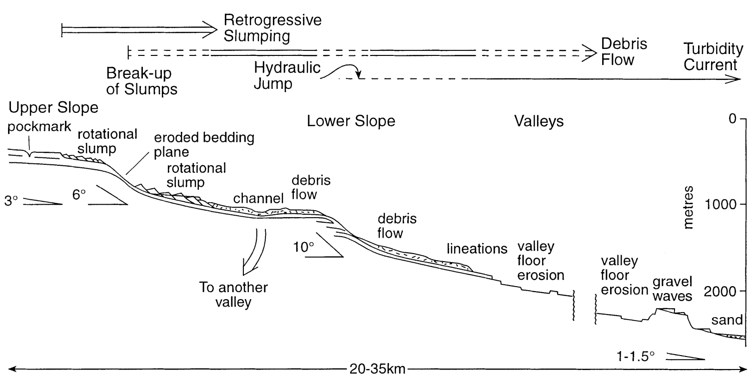

Fig. 16. Interpretative cartoon showing the sequence of sediment facies developed sequentially downslope on the St Pierre Slope and Eastern Valley. Also shown are the spatial relationships of features illustrated in SAR sidescan images and the inferred dominant sediment transport processes.

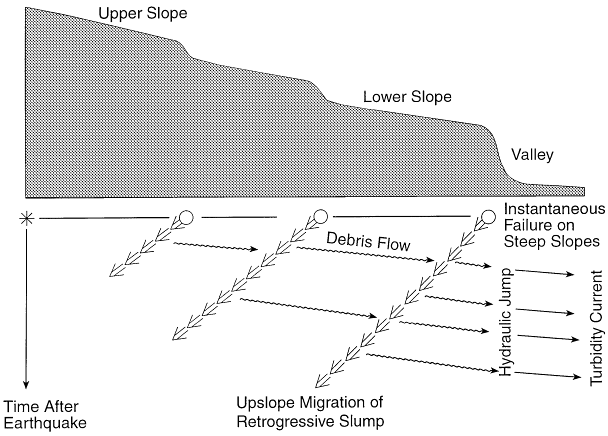

Fig. 17. Time–distance plot showing multiple failure events on steep slopes, triggering several retrogressive slumps, which then evolve into debris flows. Transformation of these flows into turbidity currents on steep slopes takes place over a period of hours.

on the continental slope (Figs 16, 17). The development of unlimited deformation of a sediment mass in failure depends on the slope (driving stress) and on the remoulded shear strength, usually undrained under marine conditions (Morgenstern, 1967). Generally, liquefaction of sediments on slopes of > 5° results in debris flows (or flow slides: Bartlett & Youd, 1992), with failure on flatter slopes tending to result in lateral spreading. Local zones of steepness on the seabed were the preferential sites of sediment failure during earthquake shaking and thus initiated retrogressive slumping. On steeper slopes, failure resulted in debris flows.

Provided that retrogression of slumps in cohesive sediment is relatively slow, slumping has the potential to provide sediment to debris flows over a period of many hours or even days. On land, the rate of retrogression in sensitive clays is of the order of 3 km h^{-1} and in non-sensitive clays it is much less (Bentley & Smalley, 1984, p. 466). Extensive areas of exposed bedding planes (e.g. the north-eastern ends of Figs 10 and 11) may be the result of surface sloughing of the type described by Sangrey & Paul (1971). On land, Mitchell & Markell (1974) suggest that flowslides that involve retrogression of more than about 10 times the scarp height involve principally plastic flow and develop into mudflows. Some mudflows in landslides zones on land move at rates of less than a metre per day, although these may be drained and therefore not completely comparable (Brunsden, 1984). Debris flows are, of course, much more rapid (velocities measured in km h^{-1}).

Alternatively, the delayed response to earthquake shaking may have been less regular and a consequence of inertial effects during shaking. In several cases on land (e.g. Superstition Hills failure, San Fernando Dam failure: Gu *et al.*, 1993, 1994), deformation began hours or even days after earthquake shaking ended. In these cases, the process is thought to involve collapse of the sediment framework, transfer of shear stress to the porewater, and then time-dependent stress redistribution to zones of inherent weakness, permitting retrogressive failure.

Steep slopes between zones of debris flow deposits and the main valleys that incise the continental slope appear to have provided the opportunity for debris flows to transform into turbidity currents, perhaps in places as a result of a hydraulic jump. Downslope evolution of the turbidity current through the process of ignition resulted in the erosion of pre-existing sand and gravel on the valley floors, as demonstrated by Hughes Clarke *et al.* (1990).

CONCLUSIONS

1 Sediment failure around the epicentre of the 1929 Grand Banks earthquake shows a downslope transition from retrogressive rotational slumps, through debris flows, to erosional features inferred to have been cut by turbidity currents. Many morphological features described from landslides and debris flows on land are recognized.

2 There is no evidence that the 1929 turbidity current resulted from a large or deep-seated failure. Rather, it was triggered by numerous relatively small thin-skinned failures. The retrogression of these numerous successive overlapping slumps led to a large translational slide.

3 Zones of local increase in slope were important in the evolution of the 1929 turbidity current. Retrogressive slumps were initiated on such steep zones. They subsequently became the sites at which slumps broke up into debris flows, and debris flows passed through hydraulic jumps into turbidity currents.

4 Prolonged or delayed retrogressive slumping and evolution of this failed material on local steep slopes provides a mechanism for nourishing a sustained turbidity current over a period of many hours.

ACKNOWLEDGEMENTS

Fieldwork was carried out under a cooperative programme between IFREMER and the Atlantic Geoscience Centre and was partly funded by the Canada Program for Energy Research and Development. M.L.M. was supported by the Natural Sciences and Engineering Research Council. We thank our shipboard colleagues including the SAR team and the Master, officers and crew of the C.S.S. Hudson. SAR images were processed by Eliane LeDrezen. The manuscript was improved by reviews by Harold Christian, Ken Skene, Bruno Savoye, Phil Hill and Reinhard Hesse. This is Geological Survey of Canada contribution 1996412.

REFERENCES

Allen, J.R.L. (1971) Mixing at turbidity current heads and its geological implications. *J. Sedim. Petrol.*, **41,** 97–113.

Augustin, J.M. and Voisset, M. (1989) Images sonar et cartographie en géologie. *Imagerie Vision Lateral*, **69,** 20–27.

Bartlett, S.F. and Youd, T.L. (1992). *Empirical Prediction of Horizontal Ground Displacement Generated by Liquefaction-Induced Lateral Spread.* National Center for Earthquake Engineering Research, Technical Report NCEER 92-0021.

Bentley, S.P. and Smalley, I.J. (1984) Landslips in sensitive clay. In: *Slope Instability* (Ed. by D. Brunsden and D.B. Prior), pp. 457–490. Wiley, Chichester.

Bonifay, D. and Piper, D.J.W. (1988) Probable Late Wisconsinan ice margin on the upper continental slope off St. Pierre Bank, eastern Canada. *Can. J. Earth Sci.*, **25,** 853–865.

Brunsden, D. (1984) Mudslides. In: *Slope Instability* (Ed. by D. Brunsden and D.B. Prior), pp. 363–418, Wiley, Chichester.

Cochonat, P. and Piper, D.J.W. (1995) Source area of sediments contributing to the 'Grand Banks' 1929 turbidity current. In: *Atlas of Deep Water Environments: Architectural Style in Turbidite Systems* (Ed. by K.T. Pickering, R.N. Hiscott, N.H. Kenyon, F. Ricci Lucchi and R.D.A. Smith), pp. 12–13. Chapman & Hall, London.

Doxsee, W.W. (1948) The Grand Banks earthquake of November 18, 1929. *Publ. Dominion Observ. Ottawa*, **7,** 323–335.

Gu, W.H., Morgenstern, N.R. and Robertson, P.K. (1993). Progressive failure of lower San Fernando Dam. *J. Geotech. Eng.*, **119,** 333–349.

Gu, W.H., Morgenstern, N.R. and Robertson, P.K. (1994). Postearthquake deformation analysis of Wildlife Site. *J. Geotech. Eng.*, **120,** 274–289.

Hampton, M.A. (1972) The role of subaqueous debris flow in generating turbidity currents. *J. Sedim. Petrol.*, **42,** 775–793.

Heezen, B.C. and Ewing, M. (1952). Turbidity currents and submarine slumps and the 1929 Grand Banks earthquake. *Am. J. Sci.*, **250,** 849–873.

Hesse, R. and Klaucke, I. (1995) A continuous along-slope seismic profile from the Upper Labrador Slope. In: *Atlas of Deep Water Environments: Architectural Style in Turbidite Systems* (Ed. by K.T. Pickering, R.N. Hiscott, N.H. Kenyon, F. Ricci Lucchi and R.D.A. Smith), pp. 18–22. Chapman & Hall, London.

Hughes Clarke, J.E. (1987) Surficial geology of Eastern Valley, Laurentian Fan. *Geol. Surv. Canada Open File* 1425.

Hughes Clarke, J.E. (1988) *The Geological Record of the 1929 'Grand Banks' Earthquake and its Relevance to Deep-Sea Clastic Sedimentation.* PhD Thesis, Dalhousie University, Halifax, Nova Scotia.

Hughes Clarke, J.E. (1990) Late stage slope failure in the wake of the 1929 Grand Banks earthquake. *Geo-Marine Lett.*, **10,** 69–80.

Hughes Clarke, J.E., Mayer, L.A., Piper, D.J.W. and Shor, A.N. (1989) Pisces IV submersible operations in the epicentral region of the 1929 Grand Banks earthquake. *Geol. Surv. Canada Paper*, **88-20,** 57–69.

Hughes Clarke. J.E., Shor, A.N., Piper, D.J.W. and Mayer, L.A. (1990). Large-scale current-induced erosion and deposition in the path of the 1929 Grand Banks turbidity current. *Sedimentology*, **37,** 613–629.

Johnson, A.M. and Rodine, J.R. (1984). Debris flow. In: *Slope Instability* (Ed. by D. Brunsden and D.B. Prior), pp. 257–361. Wiley, Chichester.

Kirwan, A.D. Jr, Doyle, L.J., Bowles, W.D. and Brooks, G.R. (1986) Time-dependent hydrodynamic models of turbidity currents analyzed with data from the Grand Banks and Orleansville events. *J. Sedim. Petrol.*, **56,** 379–386.

Mitchell, R.J. and Markell, A.R. (1974) Flowsliding in sensitive soils. *Can. Geotech. J.*, **11,** 11–31.

Morgenstern, N.R. (1967) Submarine slumping and the initiation of turbidity currents. In: *Marine Geotechnique* (Ed. by A.F. Richards), pp. 189–220. University of Illinois Press, Urbana, Illinois.

Mulder, T. and Cochonat, P. (1996) Classification of offshore mass movements. *J. Sedim. Res.*, **66,** 43–57.

Mulder, T., Berry, J.A. and Piper, D.J.W. (1997) Links between morphology and geotechnical characteristics of large debris flow deposits in the Albatross area on the Scotian Slope (SE Canada). *Marine Geotech.*, **15,** 253–281.

Parker, G. (1982) Conditions for the ignition of catastrophically erosive turbidity currents. *Marine Geol.*, **46,** 307–327.

Piper, D.J.W. (1988) Glaciomarine sediments on the continental slope off eastern Canada. *Geosci. Can.*, **15,** 23–28.

Piper, D.J.W. and Aksu, A.E. (1987) The source and origin of the 1929 Grand Banks turbidity current inferred from sediment budgets. *Geo-Marine Lett.*, **7,** 177–182.

Piper, D.J.W. and Normark, W.R. (1989) Late Cenozoic sea-level changes and the onset of glaciation: impact on continental slope progradation off eastern Canada. *Marine Petrol. Geol.*, **6,** 336–348.

Piper, D.J.W., Shor, A.N., Farre, J.A., O'Connell, S. and Jacobi, R. (1985) Sediment slides around the epicenter of the 1929 Grand Banks earthquake. *Geology*, **13,** 538–541.

Piper, D.J.W., Shor, A.N. and Hughes Clarke, J.E. (1988) The 1929 Grand Banks earthquake, slump and turbidity current. In: *Sedimentological Consequences of Convulsive Geologic Events* (Ed. by H.E. Clifton), *Geol. Soc. Am. Special Paper* **229,** 77–92.

Piper, D.J.W., Cochonat, P., Ollier, G., LeDrezen, E., Morrison, M. and Baltzer, A. (1992) Evolution progressive d'un glissement rotational vers un courant de turbidité: cas du séisme de 1929 des Grands Bancs. *C. R. Acad. Sci. Paris*, **314,** 1057–1064.

Sangrey, D.A. and Paul, M.J. (1971) A regional study of landsliding near Ottawa. *Can. Geotech. J.*, **8,** 315–335.

Shanmugam, G. (1996) High-density turbidity currents: are they sandy debris flows? *J. Sedim. Res.*, **66,** 2–10.

Shanmugam, G., Bloch, R.B., Mitchell, S.M., Beamish, G.W., Hodgkinson, R.J., Damuth, J.E., Straune, T., Syvertsen, S.E. and Shiels, K.E. (1995) Basin-floor fans in the North Sea: sequence stratigraphic models vs. sedimentary facies. *AAPG Bull.*, **79,** 477–512.

Shor, A.N., Piper, D.J.W., Hughes Clarke, J. and Mayer, L.A. (1990) Giant flute-like scour and other erosional features formed by the 1929 Grand Banks turbidity current. *Sedimentology,* **37,** 631–645.

Skempton, A.W. and Hutchinson, J.N. (1969) Stability of natural slopes and embankment foundations: state-of-the-art report. In: *Proceedings of the 7th International Conference on Soil Mechanics and Foundation Engineering,* Volume 2, pp. 291–335.

Weirich, F.H. (1989) The generation of turbidity currents by subaerial debris flows, California. *Geol. Soc. Am. Bull.*, **101,** 278–291.

Manuscript received 28 November 1996;
revision accepted 27 March 1998.